Light: Science & Applications (2015) 4, e261; doi:10.1038/lsa.2015.34
© 2015 CIOMP. All rights reserved 2047-7538/15
www.nature.com/lsa

ORIGINAL ARTICLE

# Synthetic aperture-based on-chip microscopy

**Wei Luo[1,2,3,*], Alon Greenbaum[1,2,3,*], Yibo Zhang[1,2,3] and Aydogan Ozcan[1,2,3,4]**

**Wide field-of-view (FOV) and high-resolution imaging requires microscopy modalities to have large space-bandwidth products. Lensfree on-chip microscopy decouples resolution from FOV and can achieve a space-bandwidth product greater than one billion under unit magnification using state-of-the-art opto-electronic sensor chips and pixel super-resolution techniques. However, using vertical illumination, the effective numerical aperture (NA) that can be achieved with an on-chip microscope is limited by a poor signal-to-noise ratio (SNR) at high spatial frequencies and imaging artifacts that arise as a result of the relatively narrow acceptance angles of the sensor's pixels. Here, we report, for the first time, a synthetic aperture-based on-chip microscope in which the illumination angle is scanned across the surface of a dome to increase the effective NA of the reconstructed lensfree image to 1.4, achieving e.g., ~250-nm resolution at 700-nm wavelength under unit magnification. This synthetic aperture approach not only represents the largest NA achieved to date using an on-chip microscope but also enables color imaging of connected tissue samples, such as pathology slides, by achieving robust phase recovery without the need for multi-height scanning or any prior information about the sample. To validate the effectiveness of this synthetic aperture-based, partially coherent, holographic on-chip microscope, we have successfully imaged color-stained cancer tissue slides as well as unstained Papanicolaou smears across a very large FOV of 20.5 mm$^2$. This compact on-chip microscope based on a synthetic aperture approach could be useful for various applications in medicine, physical sciences and engineering that demand high-resolution wide-field imaging.**
*Light: Science & Applications* (2015) **4,** e261; doi:10.1038/lsa.2015.34; published online 27 March 2015

**Keywords:** computational imaging; lensfree microscopy; on-chip microscopy; synthetic aperture

## INTRODUCTION

Wide field-of-view (FOV) and high-resolution imaging is crucial for various applications in biomedical and physical sciences. Such tasks demand microscopes to have large space-bandwidth products (SBPs) with minimal spatial aberrations that distort the utilization of the SBP of the imaging system. Conventional lens-based digital microscopes can achieve high-resolution imaging over a large FOV using mechanical scanning stages to capture multiple images from different parts of the specimen that are digitally stitched together. This scanning approach, however, demands a relatively bulky and expensive imaging set-up. In contrast, recent advances in digital components and computational techniques have enabled powerful imaging methods,[1–10] and when these are combined with state-of-the-art image sensor technology, it has made lenses unnecessary in certain microscopic imaging tasks.[11–17] For example, by taking advantage of image sensor chips with large mega-pixels, small pixel pitch and low cost, lensfree holographic on-chip microscopy provides unique opportunities for achieving ultra-large SBP within a cost-effective and compact imaging design.[18–20] Using source-shifting-based pixel super-resolution techniques,[18,21] lensfree on-chip imaging achieves submicrometer resolution over a wide FOV of 20–30 mm$^2$, providing gigapixel throughput with a simple, compact and unit-magnification design.[22–24] This computational imaging technique reconstructs not only the amplitude, but also the phase information of the specimen, revealing its optical path length distribution. For robust recovery of this phase information, previous lensfree on-chip imaging approaches adopted a multi-height approach,[20] which captures diffraction patterns of the sample at different sample-to-sensor distances.[25–29]

To maintain a high numerical aperture (NA) and improved resolution across the entire visible spectrum, some of the major challenges that on-chip microscopy faces include signal-to-noise ratio (SNR) deterioration and aberrations that affect the high spatial frequencies of the sample. The physical origin of the challenge of detecting high spatial frequencies on a chip is related to the relatively narrow angular response and large pixel size of opto-electronic image sensor chips. This effect becomes much worse at longer illumination wavelengths because the diffraction angles of a given high spatial frequency band increase with wavelength. Although computational approaches involving pixel super-resolution[18,21] and pixel function estimation or measurement[23] can partially help to boost some of these spatial frequencies, on-chip microscopy has thus far been limited to an NA of less than about 0.8–0.9.[11,23,30]

Synthetic aperture approaches in optical microscopy[31–45] were originally implemented to overcome the limited SBPs of traditional lens-based imaging designs. Here, we demonstrate the first application of the

[1]Electrical Engineering Department, University of California, Los Angeles, CA 90095, USA; [2]Bioengineering Department, University of California, Los Angeles, CA 90095, USA; [3]California NanoSystems Institute (CNSI), University of California, Los Angeles, CA 90095, USA and [4]Department of Surgery, David Geffen School of Medicine, University of California, Los Angeles, CA 90095, USA
*These authors contributed equally to this work
Correspondence: A Ozcan, 420 Westwood Plaza, Engr. IV 68-119, UCLA, Los Angeles, CA 90095, USA
E-mail: ozcan@ucla.edu
Received 9 August 2014; revised 20 December 2014; accepted 22 December 2014; accepted article preview online 23 December 2014

synthetic aperture technique in lensfree holographic on-chip imaging to reach a record high NA of 1.4 over a large FOV of >20 $mm^2$, where the sample is sequentially illuminated at various angles using a partially coherent light source (Figure 1). In this approach, which we term LISA (lensfree imaging using synthetic aperture), at each hologram recording process using an oblique illumination angle, some of the higher spatial frequencies that are normally attenuated or missed by the sensor chip are shifted to lower spatial frequencies (Figure 2) where the pixel response is significantly improved. This frequency shifting process due to angular diversity in illumination could also enable some of the evanescent waves that would normally never reach the sensor chip to be converted to travelling waves, permitting the digital synthesis of an NA that is larger than the refractive index of air or the medium between the sample and the sensor planes (Figure 3).

In addition to achieving the largest NA reported for on-chip microscopy, combining the information acquired at different illumination angles also significantly improves the overall SNR of the spatial frequency map of the sample, which permits robust phase recovery even for dense and connected samples, such as histopathology slides, without the need for multi-height scanning[20] or any prior information about the specimen/object.[46,47] To demonstrate LISA's success in complex wave retrieval, we performed lensfree color imaging of breast cancer tissue samples stained with hematoxylin and eosin over a very large FOV of 20.5 $mm^2$, which is equal to the active area of the sensor chip (Figures 4 and 5). Furthermore, we achieved high-resolution imaging of unlabeled biological samples, such as unstained Papanicolaou (Pap) smears (Figure 6). Such unstained pathology samples do not exhibit sufficient contrast in intensity and are therefore difficult to observe unless phase contrast objective-lenses and special illumination schemes are used. With LISA, however, these unstained samples can be imaged using the reconstructed phase information without a change in either the imaging set-up or the reconstruction algorithm.

Compared to other applications of synthetic aperture techniques in microscopy,[31–45] LISA has important advantages in terms of a significantly wider FOV, simplicity and compactness of the imaging set-up and could be quite useful for various biomedical and physical sciences related applications that demand high-resolution and large FOV microscopic imaging.

## MATERIALS AND METHODS

### Experimental set-up

In our set-up (Figure 1), a broadband light source (WhiteLase-Micro; Fianium Ltd, Southampton, UK) is filtered using an acousto-optic tunable filter and then coupled into a single mode optical fiber to provide partially coherent and tunable illumination of the specimen. The spectral bandwidth of the light coming out of the fiber is approximately 2.5 nm, and the power of the illumination is ~20 μW. The illumination fiber is mounted on a rotational arm whose axis of

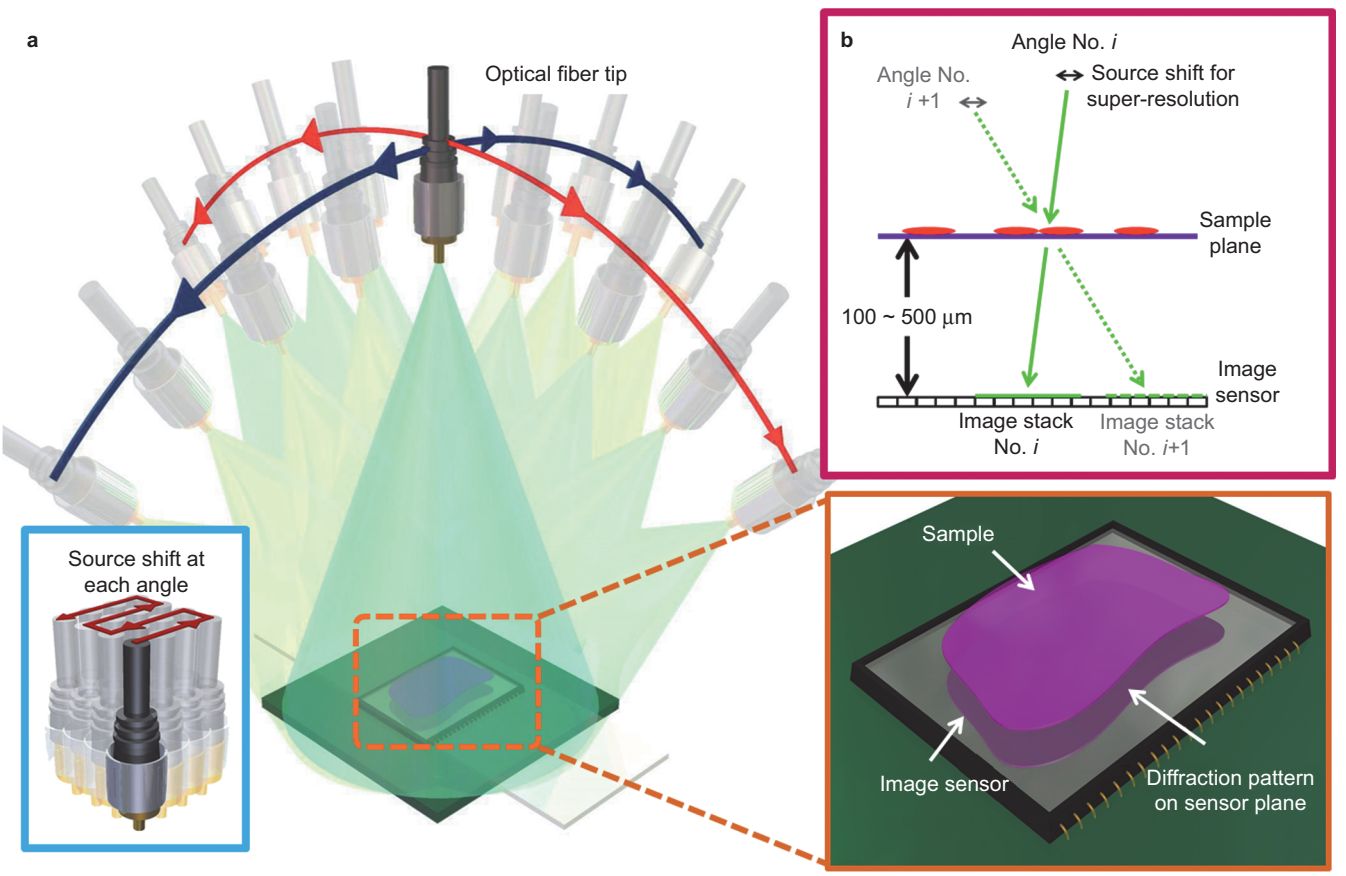


**Figure 1** LISA experimental set-up. (**a**) A partially coherent light source (spectral bandwidth: ~2.5 nm) is coupled to a single mode fiber. This fiber is mounted on a rotational arm to provide tilted illumination across two orthogonal axes (red and blue trajectories). At each angle, the source is laterally shifted multiple times (see bottom left inset) to capture a stack of lower-resolution holographic images. (**b**) The sample is placed onto the image sensor chip at a distance of about 100–500 μm. Both the sample-to-sensor distances and illumination angles are automatically calculated using computational methods, thus eliminating the need for complicated mechanical calibration procedures. LISA, Lensfree Imaging using Synthetic Aperture.


doi:10.1038/lsa.2015.34

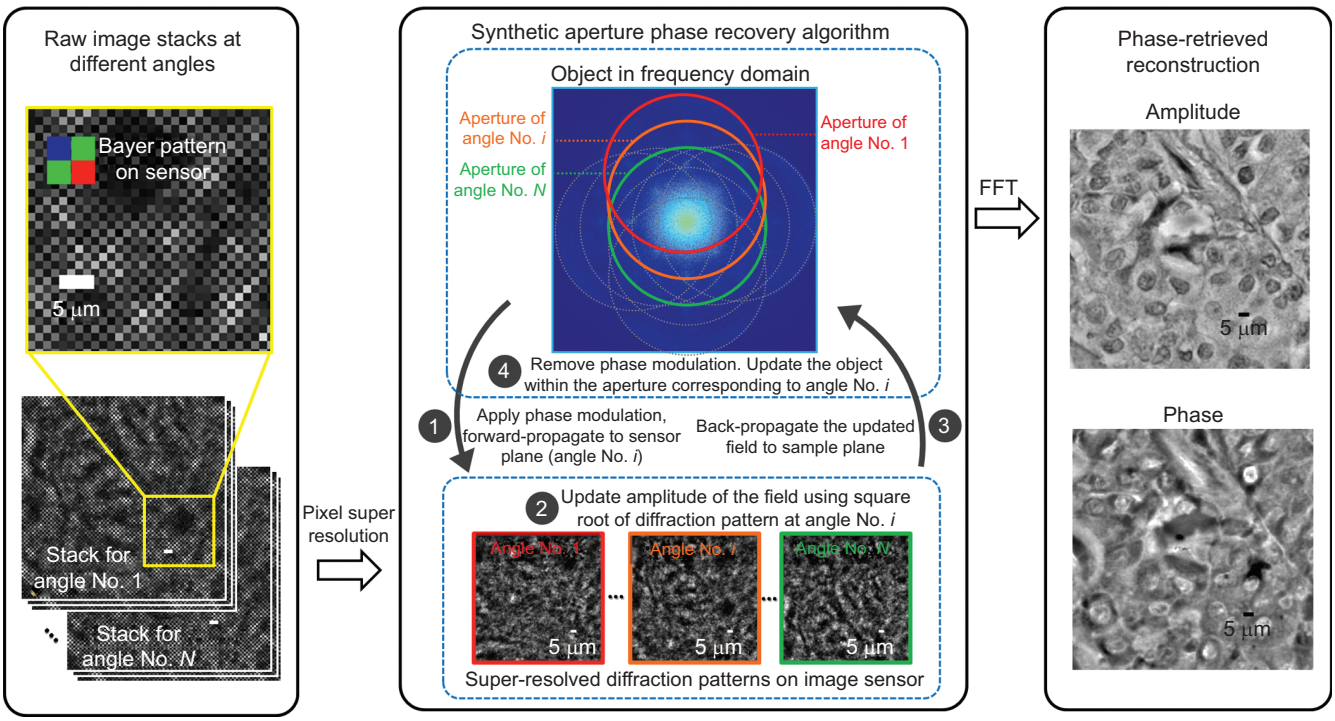


**Figure 2** Reconstruction algorithm of lensfree on-chip imaging using the synthetic aperture approach. The pixel super-resolution algorithm uses lensfree lower-resolution images (left column) captured at different illumination angles (No. 1 through No. *N*) to synthesize pixel super-resolved in-line holograms. Middle: a four-step iterative process for synthetic aperture and phase retrieval, which is repeated for all the illumination angles. As an example, for a human breast tissue sample, the reconstruction of the complex sample field can be obtained (right column) after 5–10 cycles using 22 different illumination angles (−50° to 50° at 10° increments along two orthogonal axes). FFT, fast Fourier transform.

rotation is aligned within the plane of the image sensor chip (1.12-μm pixel-pitch CMOS (complementary metal oxide semiconductor) color sensor; Sony Corp, Tokyo, Japan). The distance between the fiber end and the image sensor is about 7–11 cm. The rotational arm is installed on a set of linear stages that provide a lateral light source shift that is used for pixel super-resolution. The CMOS image sensor is also installed on a rotation mount so that the sensor can be rotated within a lateral plane. During the data acquisition process, source shift, angle tilt and image acquisition are all automated and coordinated by custom-written LabVIEW software.

### Pixel super-resolution

To digitally mitigate under-sampling artifacts and consequently improve LISA's spatial resolution, pixel super-resolution is implemented. During the lensfree image acquisition at each angle, the light source is shifted laterally by small amounts (e.g., about 0.1–0.2 mm), and a raw diffraction pattern is sequentially captured at each light source position. Note that these sub-pixel lateral shifts are negligible compared to the source-to-sample distance (e.g., about 7–11 cm), and therefore, the illumination angle remains approximately constant during the pixel super-resolution data acquisition. These sub-pixel shifts allow us to synthesize a high-resolution in-line hologram for each angle using multiple (typically 16–64) lower-resolution in-line holograms.[18,21,48–51] In the synthesis of the super-resolved holograms, the responsivity distribution within the pixel is also taken into account to compensate for the attenuation of the specimen's high frequency components, as detailed in Ref. 23. In a typical lensfree synthetic aperture experiment, images from two orthogonal illumination axes are acquired at 10° increments spanning from −50° to +50°.

### Autofocus algorithm

An autofocus algorithm is implemented to digitally estimate the sample-to-sensor distance as well as the illumination angle, which will be detailed in the next sub-section. For sample-to-sensor distance estimation, the super-resolved hologram from the lowest illumination angle is back-propagated to different planes; in each plane, the algorithm evaluates the sharpness of the resulting image, which is defined as the variance of the gradient of the image, calculated using Sobel operators.[22,52] The plane with the highest sharpness is selected as the object plane.

### Computational calibration of the illumination angle

In our set-up, a rotation arm is used to vary the illumination angle. This rotation arm is inaccurate and can cause up to 4° discrepancies between experiments. However, our iterative synthetic aperture and phase retrieval algorithm requires accurate angle information, since such errors would result in a loss of spatial resolution and phase convergence problems. Toward this end, we devised a three-step computational method to automatically calibrate the illumination angles. First, the sample-to-sensor distance is evaluated using an autofocus algorithm, as detailed in the previous sub-section. For this purpose, a hologram, which is captured at an approximately normal illumination angle, is utilized. Second, given the calculated sample-to-sensor distance, an 'angular autofocus algorithm' is used to accurately find the illumination angle that is associated with one of the measurements. This algorithm receives one super-resolved hologram as input, which is captured with an oblique illumination angle, and an initial guess for the illumination angle based on the rotational arm position. The algorithm then back-propagates the hologram while scanning the illumination angles at 0.1°

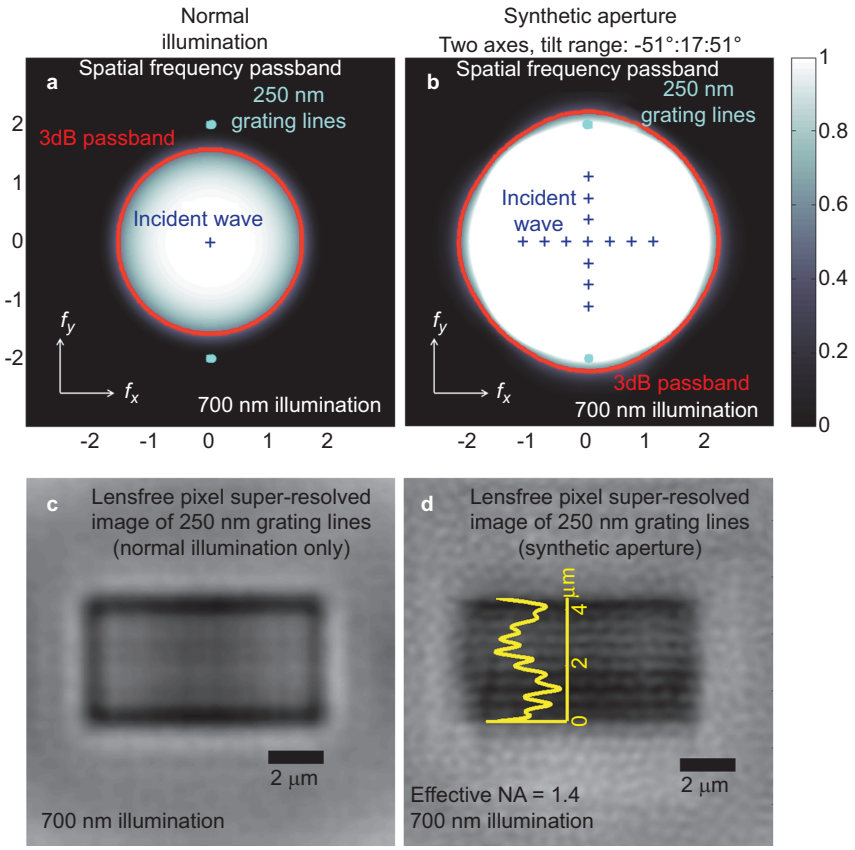


**Figure 3** Our synthetic aperture approach enables lensfree on-chip imaging to reach a numerical aperture of 1.4. (**a**, **b**) The imaging system passbands in the spatial frequency domain, without and with the synthetic aperture, respectively. (**c**, **d**) Lensfree amplitude images of 250 nm grating lines without and with the iterative synthetic aperture reconstruction algorithm, respectively. The spatial frequencies of the grating lines are marked by cyan dots in **a** and **b**. To reconstruct the image in **d**, illumination angles of −51°:17:51° across two axes are used ($\lambda$=700 nm), and four iterations, as described in Figure 2, were sufficient to achieve convergence. Note that the sample-to-sensor distance is ~100 μm. FFT, fast Fourier transform.

increments spanning from −4° to +4° around the initial illumination angle estimate. The algorithm calculates the edge sharpness for each resulting image, and the angle that corresponds to the maximum sharpness is selected to be the correct illumination angle for this hologram. After finding the absolute illumination angle for one hologram (i.e., the 'anchor' hologram), the rest of the illumination angles can be found by finding the shifts of the rest of the super-resolved holograms relative to the 'anchor' hologram.

### Iterative synthetic aperture-based phase recovery

The iterative phase recovery process enables the reconstruction of connected and dense specimens by reconstructing the phase of the optical wave. The algorithm receives as input $N$ pixel super-resolved holograms that are synthesized from $N$ different illumination angles and an initial guess of the specimen. This initial guess can be generated by simply back-propagating the hologram at one of the illumination angles using the angular spectrum approach.[53] Alternatively, the initial guess can be generated by summing the back-propagation results from multiple angles. Then, a four-step iterative process is carried out to perform synthetic aperture-based phase retrieval (Figure 2). First, the initial guess, i.e., a complex field representing the specimen, is forward-propagated to the sensor plane. Before the propagation, a phase modulation is applied, which is determined by the illumination angle that is selected. Due to our lensfree and unit magnification configuration, we can simply use a flat-top filter as the forward-propagation aperture. Second, the amplitude of the forward-propagated field is updated using the square root of the diffraction pattern measured at this angle (updated using a weighted average: ~60% of the newly forward-propagated field and ~40% of the measured one). Third, this updated field on the sensor plane is back-propagated to the sample plane, and the phase modulation is removed. Fourth, in the frequency domain, a sub-region, i.e., an aperture, is updated (also using a weighted average, as detailed above) using the back-propagated complex field from step three. The center of this aperture is determined by the illumination angle, and the boundary of this aperture is defined as where the signal attenuation is equal to 3 dB. In our set-up, 22 angles (e.g., −50° to 50° at 10° increments along two orthogonal axes) and five iteration cycles are typically utilized to achieve phase retrieval. The entire reconstruction algorithm, including pixel super-resolution and synthetic aperture phase retrieval, is implemented using MATLAB on a 3.60-GHz CPU (central processing unit) computer (Intel Xeon E5-1620, 16 GB random-access memory). For a 1×1 mm$^2$ sub-region, the reconstruction time is 46 min. During this reconstruction process, neither GPUs (graphics processing units) nor parallel computing were used. This reconstruction time could be considerably reduced by a factor of for example ~20 by implementing the algorithm using the C language on GPUs[14]; refer to the section on 'Results and discussion'.

### Digital colorization of lensfree on-chip images

Lensfree amplitude images reconstructed at three wavelengths (472 nm, 532 nm and 632 nm) are converted into intensity maps and then combined to form lensfree color (RGB) images of the sample.[20,54] During


doi:10.1038/lsa.2015.34

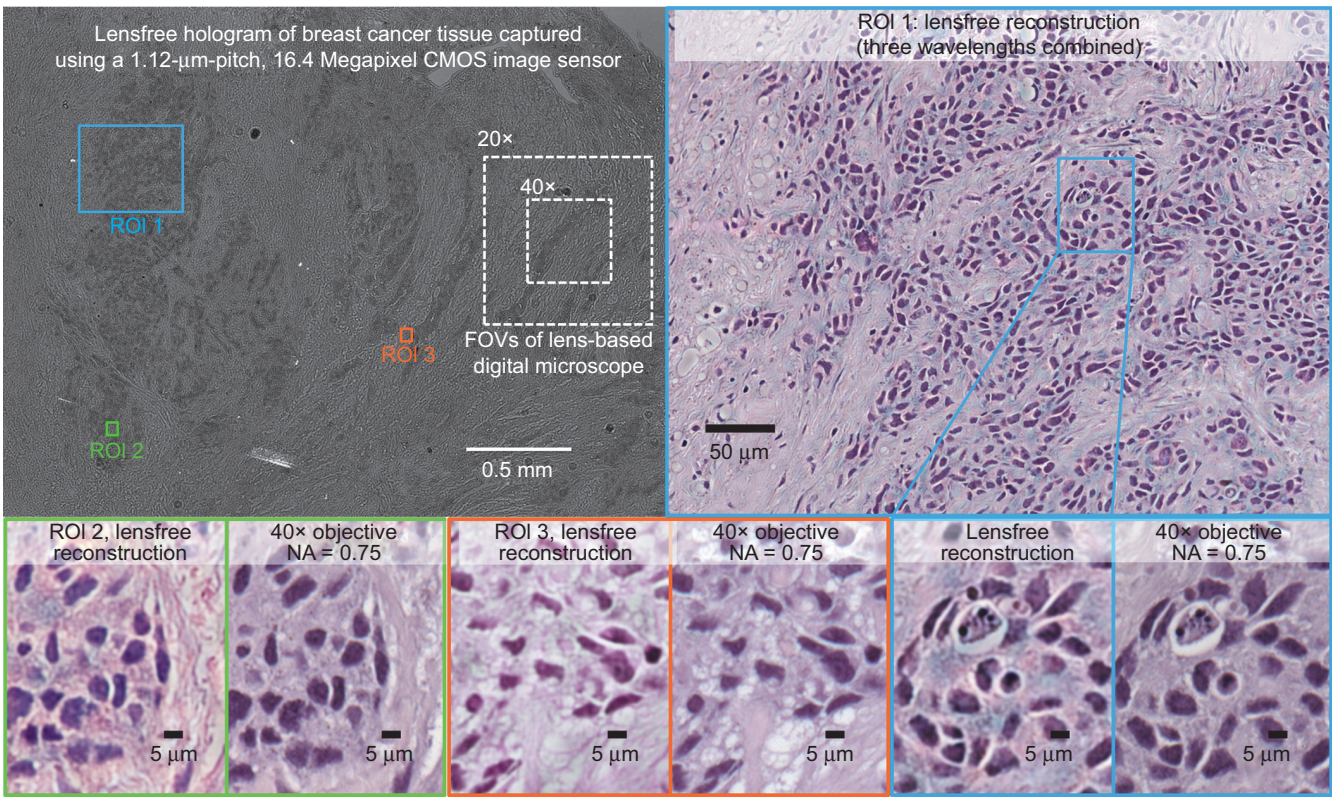


**Figure 4** Lensfree color imaging of breast cancer tissue (H&E staining) using LISA. Top left: sub-region of a lensfree hologram captured by a CMOS sensor chip; FOVs of 20× and 40× microscope objective lenses are also shown for comparison (white dashed squares). Top right: lensfree reconstruction of ROI No. 1. Bottom: zoomed images of lensfree reconstructions of various regions within the large reconstructed FOV. Conventional microscope images (40× objective, NA=0.75) are also provided for comparison. To create the lensfree color image, on-chip holographic images at three different illumination wavelengths were used ($\lambda$=472 nm, 532 nm, 632 nm). The sample-to-sensor distance is ~255 μm. FOV, field of view; H&E: hematoxylin and eosin; LISA, Lensfree Imaging using Synthetic Aperture; ROI, region of interest.

this process, histogram equalization is applied to each individual color channel. Such equalization imposes a monotonic global intensity transformation to the reconstructed intensity map so that the resulting color images agree with a visual inspection of the same sample using conventional lens-based microscopy tools. This intensity transformation can be obtained by minimizing the overall difference between the histograms of the reconstructed image and conventional microscope images within several sub-regions of the sample FOV. Once the transformations for all color channels are obtained, they can be applied to other regions or samples as long as the same illumination conditions apply.

Another method to create a color image is to digitally colorize a lensfree image that was reconstructed from only one illumination wavelength.[20] This second colorization method maps intensity to color based on prior knowledge of the imaged sample (see, e.g., Figure 5). This colorization method works in the YUV color space,[20,55,56] which contains three channels, the Y channel, which measures luma (brightness), and the U and V channels, which measure chrominance (color). The YUV color space can be converted to the RGB representation by a linear transformation. To map a mono-color image into a color image, the amplitude (or intensity) of the mono-color lensfree image is used as the Y channel, while the U and V channels can be inferred from the Y channel. The mapping is created by statistically learning a number of bright-field microscope color images of the same type of specimen that are also imaged by our lensfree on-chip microscope. In this training stage, the conventional microscope images are transformed to the YUV color space, and a pixel-by-pixel scan then links each Y value to its corresponding average U and V values, yielding a nonlinear mapping.[20] Before applying the mapping to the mono-color lensfree image, the brightness values of important features, such as the nuclei and the extra-cellular matrix, must be matched between the learning statistics and the to-be-colored gray-scale image. This can be done either by manually picking features of interest or by matching histograms. We should emphasize that this learning step needs to be performed only once for each sample type of interest.

### Digital phase contrast in lensfree on-chip imaging

Once the complex field of the sample is obtained after the phase retrieval steps, a phase shift of $\pi/2$ is digitally applied to its zero-frequency component. The intensity of this modified complex object field is then calculated to create a digital phase contrast image of the specimen (see, e.g., Figure 6).

### Sample preparation steps

The grating lines (Figure 3) used for NA and resolution quantification are fabricated on a glass substrate using focused ion beam milling. Anonymized biological samples (human breast cancer tissue in Figures 4 and 5) were purchased from the Translational Pathology Core Laboratory at UCLA. Unstained Pap smears are prepared through ThinPrep® preparation (Figure 6). All these pathology slides

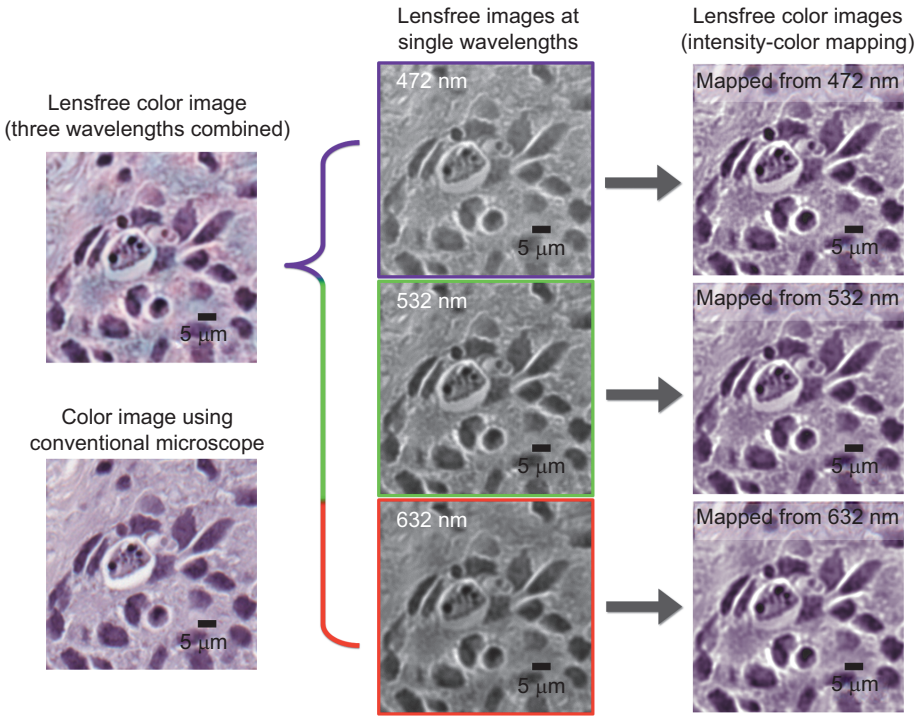


**Figure 5** Colorization methods of LISA images. Top left column: lensfree color (RGB) image generated by combining the reconstructions from three wavelengths. Bottom left column: image of the same sample taken by a conventional lens-based microscope (40× objective, NA=0.75). Center column: lensfree mono-color reconstructions at three different illumination wavelengths ($\lambda$=472 nm, 532 nm and 632 nm). Right column: lensfree color images generated by colorizing (using intensity-to-color mapping[20]) a single gray-scale image obtained using a single illumination wavelength. The specimen is a human breast cancer pathology slide. LISA, Lensfree Imaging using Synthetic Aperture; NA, numerical aperture.

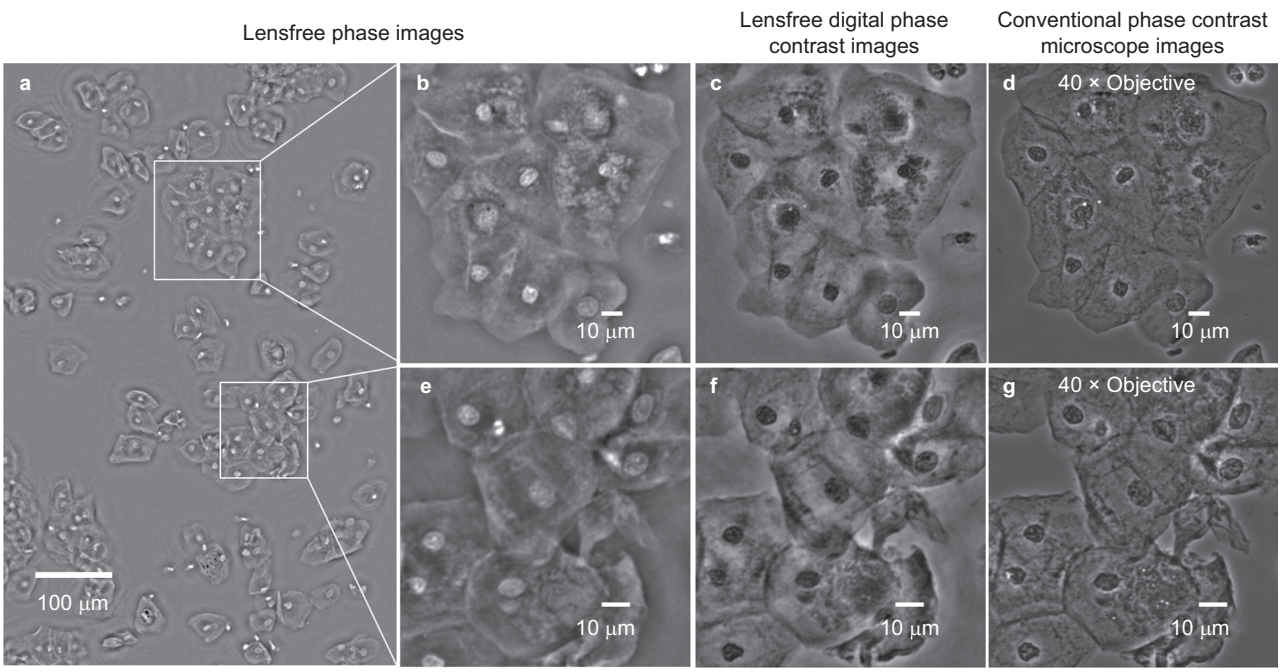


**Figure 6** LISA images of an unstained Papanicolaou smear. (**a**) A phase image of the sample obtained after six iterations of the iterative synthetic aperture reconstruction algorithm and two zoomed in regions (**b**) and (**e**). Note that with a regular lens-based microscope, these unstained cells suffer from poor contrast and could not be imaged, while the lensfree phase images reveal subcellular features of the specimen. (**c**, **f**) Lensfree digital phase contrast images processed from (**b**) and (**e**), respectively. The corresponding conventional phase contrast microscope images (**d** and **g**) using a 40× objective-lens (NA=0.75) are also provided for comparison. The sample-to-sensor distance is ~350 μm. LISA, Lensfree Imaging using Synthetic Aperture; NA, numerical aperture.


doi:10.1038/lsa.2015.34

are sealed between two glass slides. The gap between the sensor and glass slides is filled with refractive index matching oil ($n$=1.52). The sample-to-sensor distances are ~100 μm for grating lines, ~255 μm for breast cancer tissue slides and ~350 μm for Pap smear slides.

## RESULTS AND DISCUSSION

To demonstrate the NA improvement brought by LISA, 250-nm grating lines were imaged under a 700-nm illumination wavelength using the unit magnification on-chip imaging set-up shown in Figure 1. As detailed in Figure 2, the spatial sampling limitation of the sensor chip due to its 1.12-μm physical pixel pitch and unit magnification is mitigated by using source-shifting-based pixel super-resolution, which achieves an effective pixel size of 100–150 nm. The remaining major limitation on spatial resolution is the loss of SNR for high spatial frequencies, which can be addressed by the synthetic aperture approach that we have taken (see the section on 'Materials and methods'). In the frequency domain, this loss of high spatial frequency information forms a low-pass filter function (Figure 3a). Tilting the illumination angle shifts the passband of the imaging system to a new sub-region, allowing higher spatial frequencies to be detected by the image sensor (Figure 3b). By digitally combining lensfree holographic measurements obtained at different illumination angles (see Figure 2 and the section on 'Materials and methods'), we obtain the two-dimensional image of the object (Figure 3d) with a significantly broadened spatial bandwidth, as shown in Figure 3b. Figure 3d illustrates our lensfree reconstruction results based on this synthetic aperture approach, clearly resolving 250-nm grating lines under 700-nm illumination wavelength, which effectively corresponds to an NA of 1.4, i.e., 700 nm/(2×250 nm), much larger than earlier on-chip imaging results using similar sensor chips.[23] In this reconstruction result, the reduced modulation depth that is observed toward the edges can be partially attributed to the three-dimensional structure of the fabricated grating, where focused ion beam milling-induced structures at the edges start to fall out of the reconstructed depth due to our high NA. Because resolution and FOV are decoupled in our on-chip imaging set-up (Figure 1), this large numerical aperture also comes with a large FOV of 20.5 $mm^2$, which constitutes the active area of the sensor chip.

Next, to demonstrate the significantly improved phase recovery performance of LISA, as well as its accurate color rendering capability, we imaged connected tissue samples (i.e., hematoxylin and eosin-stained breast cancer tissue) over a wide FOV, as illustrated in Figure 4. During the image acquisition process, we sequentially imaged these pathology samples at three distinct wavelengths (472 nm, 532 nm and 632 nm) to digitally generate a lensfree color (i.e., RGB) image of the specimen.[20,54] LISA's color images (see Figure 4 and the section on 'Materials and methods' for details) show very good agreement with 40× microscope objective images of the same specimen. To boost the data acquisition speed, we further demonstrated that lensfree color imaging capability can also be achieved by transforming the intensity channel of a holographically reconstructed image acquired at a single wavelength[20] into a pseudo-color image (Figure 5). This intensity-to-color transformation, as successfully demonstrated in Figure 5, can be statistically established and fine-tuned based on prior knowledge of the sample type, as well as the stain of interest, and can provide a rapid solution for digital colorization of lensfree holographic images without the need to perform multi-wavelength illumination of the specimen.

To demonstrate the label-free imaging capabilities of LISA, we also imaged unstained Pap smear slides, as illustrated in Figure 6. Imaging this type of transparent and unlabeled samples usually requires adding a special objective lens and/or illumination module to a conventional microscope to convert optical path differences into brightness variations. With LISA, no additional components or modification in the reconstruction algorithm are needed because LISA inherently reconstructs both the amplitude and phase information of the specimen. In addition to directly visualizing the phase image of the specimen, as illustrated in Figure 6b and 6e, we can also digitally replicate the physical image formation process of a phase contrast microscope.[57] For example, a phase shift of $\pi/2$ can be added to the zero frequency component of the complex field, and the intensity of this new field mimics a phase contrast image, as seen in Figure 6c and 6f. These lensfree images provide decent agreement with images of the same sample taken by an actual phase contrast microscope using a 40× (NA=0.75) objective lens.

In lensfree on-chip microscopy, the characteristic signature is unit magnification, where the FOV and resolution are decoupled, setting the active area of the sensor array as the sample FOV. While these features are highly desirable for creating high-throughput and compact on-chip microscopy systems, they also create two major problems, both of which are related to the pixels of the sensor array: first, spatial undersampling due to large pixel size (e.g., 1–2 μm) and, second, poor SNR and aberrations experienced by high spatial frequencies due to the narrow pixel acceptance angle and the opto-electronic hardware in front of the active region of the pixels. Pixel super-resolution approaches[18,21] mitigate the first challenge due to large pixel size by, e.g., source shifting, which creates sub-pixel shifted replicas of the diffraction patterns of the samples on the sensor array, and these can be utilized to digitally divide each pixel into smaller effective pixels, undoing the effects of spatial undersampling. To implement pixel super-resolution, LISA uses a very small angular modulation of the source (<0.5° in our set-up) since a small shift of the source is sufficient to generate a sub-pixel shift of the in-line hologram at the sensor plane. In contrast, shadow imaging-based on-chip microscopes[17] demand very large illumination angles (e.g., ±60°) to be scanned to perform pixel super-resolution because their sample-to-sensor distances need to be sub-micron for acceptable spatial resolution. Stated differently, shadow-based on-chip microscopy utilizes angular diversity of the illumination entirely for pixel super-resolution,[17] whereas LISA uses a much smaller angular range (<0.5°) to perform pixel super-resolution and leaves the rest of the angular space in illumination to increase the effective NA using synthetic aperture. This synthetic aperture approach is essential to mitigate pixel-related aberrations and signal loss that high spatial frequencies inevitably experience in an on-chip microscope design, the effects of which become even worse at longer illumination wavelengths because the diffraction angles of a given band of high spatial frequencies increase with wavelength. Such an improvement in NA brought by LISA is critical for maintaining a competitive resolution especially at longer wavelengths, which paves the way for high resolution on-chip microscopy across the entire visible spectrum. Assuming that the partial coherence of light does not pose any resolution limitations (i.e., the spectral bandwidth and the spatial coherence of the illumination source are appropriately adjusted), this synthetic aperture-based on-chip microscope, through pixel super-resolution, can theoretically achieve an effective NA of $1+n_2$, where the medium between the source and the sample plane is assumed to be air, and $n_2 \geqslant 1$ is the refractive index of the medium between the sample and sensor planes. However, SNR degradation of the lensfree holograms, especially at oblique illumination angles and with larger sample-to-sensor distances, would create practical limitations to perform ideal pixel super-resolution and phase recovery, which would make it challenging

to reach this theoretical NA value. In fact, compared to Figure 3, the relatively lower resolution that is observed in our reconstructed LISA images in Figures 4–6 can be attributed to reduced hologram SNR and increased sample-to-sensor distances (from 100 μm in Figure 3 to 255 μm and 350 μm in Figures 4 and 6, respectively).

In addition to a significant NA increase, LISA also has a very important advantage for performing robust phase recovery, even for dense and connected tissue samples that have been difficult to reconstruct using transmission-based in-line holographic methods unless multi-height based on-chip imaging techniques are utilized.[20] The success of this phase recovery performance of LISA relies on our iterative synthetic aperture approach and is illustrated using pathology samples, as presented in Figures 4–6. It should be emphasized that this complex wave retrieval step also enables us to digitally 'focus' on the sample plane without the need for a priori knowledge of the sample-to-sensor distance. As a comparison, precise depth focusing during the imaging process is crucial for lens-based systems, especially when high-NA lenses are used, and mechanical implementation of autofocusing during the lateral scanning process can dramatically increase the complexity and cost of the imaging set-up. Moreover, for transparent samples, such as unlabeled biological tissue, depth focusing is particularly difficult using conventional microscopes unless costly additional optical components are added to the imaging system. LISA replaces such laborious processes with automated sample-to-sensor distance search and angle calibration algorithms (detailed in the 'Materials and methods' Section), which enable autofocusing of the complex optical wave on the sample plane during the reconstruction process. This is another major advantage over shadow-based on-chip microscopy; shadow-based imaging demands the same vertical gap to be sub-micron across the entire FOV,[17] which is rather difficult to satisfy in real samples. Placing the specimen directly in contact with the sensor chip surface can partially mitigate such height/depth variations for perfectly planar two-dimensional objects. However, this contact on-chip imaging approach comes with the risks of significantly heating the sample and damaging the sensor due to extreme proximity to the active region of the chip, and, more importantly, will inevitably demand very large illumination angles to perform pixel super-resolution.[17] These large illumination angles unfortunately introduce major spatial artifacts for shadow/contact imaging[17,58] because, at high illumination angles, the shadow of the specimen cannot be considered as a shifted version of the same object function, which forms the basic assumption of pixel super-resolution. Using synthetic aperture-enabled robust phase recovery, LISA mitigates these autofocusing challenges and related spatial artifacts while maintaining a simple, cost-effective and unit magnification imaging design.

Once the high-resolution complex field of the sample is recovered, various visualization methods are at the user's disposal, such as multi-wavelength-based colorization,[54] intensity-based color mapping[20] and digital phase contrast techniques (see the section on 'Materials and methods'). Compared with the intuitive method of combining reconstructions at multiple wavelengths (e.g., red, green, blue) to digitally form a color image of the sample, intensity-based color mapping/transformation[20] takes advantage of prior knowledge of the sample type and staining method to transform a lensfree mono-color intensity image into a color image (Figure 5). While such an approach could greatly reduce the data acquisition and reconstruction time, lensfree colorization using the red, green and blue channels, as illustrated in Figure 4, would generally be the optimal choice for an unknown sample of interest without prior information of staining.

To image transparent and colorless samples, instead of physically adding optical components to obtain phase contrast images, we can simply apply a digital phase shift to the zero frequency component of the holographically reconstructed complex object to mimic the physical image formation in phase contrast microscopy,[57] and the intensity of this phase-shifted field serves as the phase contrast image of the sample. Such images can be especially appealing for unstained pathology samples (see, e.g., Figure 6), as they visualize and enhance the contrast of spatial features that are difficult to observe under regular bright-field microscopes.

Although our proof-of-concept LISA system includes mechanical components such as linear stages to perform source-shifting-based pixel super-resolution and a rotational arm to vary the illumination angle, the implementation of our optical set-up can be further simplified and constructed without any moving components. As demonstrated earlier, source shifting can be performed by sequentially lighting up fibers within a bundle that are individually butt-coupled to light-emitting diodes.[18,19] Furthermore, as a result of our wide passband in the frequency domain (i.e., 2.0–3.2 $\mu m^{-1}$ in diameter), the number of illumination angles can also be reduced to, e.g., ~20 angles, further simplifying the optical set-up. Because the angle calibration is carried out during our numerical reconstruction process, precise alignment of the LISA set-up and illumination sources is not required, making the system robust even for mobile applications.

Being a computational imaging technique, LISA not only benefits from the rapid evolution in image sensor technology but also from advances in computing power; both the image sensor pixel count and CPU transistor count have exhibited exponential increases in the past decade, and such advances would provide immediate improvements to the performance of LISA in terms of larger space-bandwidth products and faster reconstructions. Parallel-computing platforms, such as GPUs and computer clusters, could also significantly increase the reconstruction speed of LISA, as our entire reconstruction algorithm is highly parallelizable. For instance, our full FOV (~20.5 $mm^2$) image reconstruction can be digitally divided into sub-regions for parallel processing, and for each sub-region, pixel super-resolution can be individually performed for different illumination angles. Our phase retrieval algorithm relies extensively on fast Fourier transform operations, which can also be significantly accelerated by using GPUs. In its current implementation, without parallel computing or GPU use, the entire image reconstruction (including pixel super-resolution and phase retrieval) for a 1 mm×1 mm sub-region takes ~46 min on a single desktop computer (Intel Xeon E5-1620) using MATLAB (see the section on 'Materials and methods'). This leaves significant room for speed improvement in our reconstructions; for example, utilization of the C language (instead of MATLAB) on a GPU could accelerate the phase recovery process by ~20-fold.[14]

## CONCLUSIONS

We demonstrated a synthetic aperture-based on-chip microscopy modality that can achieve an NA of 1.4 across a very large FOV (20.5 $mm^2$) under unit magnification and without any lenses. This wide-field on-chip microscope utilizes multiple angles of illumination to holographically synthesize the largest NA reported for an on-chip microscope and enables color imaging of tissue samples, including pathology slides, using complex wave retrieval. Its simple and compact design makes this partially coherent holographic on-chip microscopy platform highly appealing for high-resolution and wide-field imaging applications in biomedical and physical sciences.


doi:10.1038/lsa.2015.34

## ACKNOWLEDGEMENTS

The Ozcan Research Group at UCLA gratefully acknowledges the support of the Presidential Early Career Award for Scientists and Engineers (PECASE), the Army Research Office (ARO; W911NF-13-1-0419 and W911NF-13-1-0197), the ARO Life Sciences Division, the ARO Young Investigator Award, the National Science Foundation (NSF) CAREER Award, the NSF CBET Division Biophotonics Program, the NSF Emerging Frontiers in Research and Innovation (EFRI) Award, the NSF EAGER Award, Office of Naval Research (ONR), the Howard Hughes Medical Institute (HHMI), and the National Institutes of Health (NIH) Director's New Innovator Award DP2OD006427 from the Office of the Director, National Institutes of Health. This work is based on research performed in a laboratory renovated by the National Science Foundation under Grant No. 0963183, which is an award funded under the American Recovery and Reinvestment Act of 2009 (ARRA). A Greenbaum is an HHMI International Student Research Fellow at UCLA. We also acknowledge QS Wei of UCLA for his assistance with the microscopic imaging of some of our samples.

1 Brady DJ. *Optical Imaging and Spectroscopy*. Hoboken, NJ: Wiley; Massachusetts Ave, NW Washington, DC: Optical Society of America; 2009.
2 Xu W, Jericho MH, Meinertzhagen, Kreuzer HJ. Digital in-line holography for biological applications. *Proc Natl Acad Sci USA* 2001; **98**: 11301–11305.
3 Javidi B, Ferraro P, Hong SH, de Nicola S, Finizio A *et al*. Three-dimensional image fusion by use of multiwavelength digital holography. *Opt Lett* 2005; **30**: 144–146.
4 Ferraro P, Grilli S, Miccio L, Alfieri D, de Nicola S *et al*. Full color 3-D imaging by digital holography and removal of chromatic aberrations. *J Disp Technol* 2008; **4**: 97–100.
5 Rosen J, Brooker G. Non-scanning motionless fluorescence three-dimensional holographic microscopy. *Nat Photonics* 2008; **2**: 190–195.
6 Choi K, Horisaki R, Hahn J, Lim S, Marks DL *et al*. Compressive holography of diffuse objects. *Appl Opt* 2010; **49**: H1–H10.
7 Paturzo M, Merola F, Ferraro P. Multi-imaging capabilities of a 2D diffraction grating in combination with digital holography. *Opt Lett* 2010; **35**: 1010–1012.
8 Hahn J, Lim S, Choi K, Horisaki R, Brady DJ. Video-rate compressive holographic microscopic tomography. *Opt Express* 2011; **19**: 7289–7298.
9 Memmolo P, Iannone M, Ventre M, Netti PA, Finizio A *et al*. On the holographic 3D tracking of *in vitro* cells characterized by a highly-morphological change. *Opt Express* 2012; **20**: 28485–28493.
10 Zhu H, Mavandadi S, Coskun AF, Yaglidere O, Ozcan A. Optofluidic fluorescent imaging cytometry on a cell phone. *Anal Chem* 2011; **83**: 6641–6647.
11 Greenbaum A, Luo W, Su TW, Göröcs Z, Xue L *et al*. Imaging without lenses: achievements and remaining challenges of wide-field on-chip microscopy. *Nat Methods* 2012; **9**: 889–895.
12 Mudanyali O, McLeod E, Luo W, Greenbaum A, Coskun AF *et al*. Wide-field optical detection of nanoparticles using on-chip microscopy and self-assembled nanolenses. *Nat Photonics* 2013; **7**: 247–254.
13 Su TW, Xue L, Ozcan A. High-throughput lensfree 3D tracking of human sperms reveals rare statistics of helical trajectories. *Proc Natl Acad Sci USA* 2012; **109**: 16018–16022.
14 Isikman SO, Bishara W, Mavandadi S, Yu FW, Feng S *et al*. Lens-free optical tomographic microscope with a large imaging volume on a chip. *Proc Natl Acad Sci USA* 2011; **108**: 7296–7301.
15 Khademhosseinieh B, Biener G, Sencan I, Su TW, Coskun AF *et al*. Lensfree sensing on a microfluidic chip using plasmonic nanoapertures. *Appl Phys Lett* 2010; **97**: 221107.
16 Coskun AF, Sencan I, Su TW, Ozcan A. Lensless wide-field fluorescent imaging on a chip using compressive decoding of sparse objects. *Opt Express* 2010; **18**: 10510–10523.
17 Zheng G, Lee SA, Antebi Y, Elowitz MB, Yang C. The ePetri dish, an on-chip cell imaging platform based on subpixel perspective sweeping microscopy (SPSM). *Proc Natl Acad Sci USA* 2011; **108**: 16889–16894.
18 Bishara W, Sikora U, Mudanyali O, Su TW, Yaglidere O *et al*. Holographic pixel super-resolution in portable lensless on-chip microscopy using a fiber-optic array. *Lab Chip* 2011; **11**: 1276–1279.
19 Isikman SO, Bishara W, Sikora U, Yaglidere O, Yeah J *et al*. Field-portable lensfree tomographic microscope. *Lab Chip* 2011; **11**: 2222–2230.
20 Greenbaum A, Zhang Y, Feizi A, Chung PL, Luo W *et al*. Wide-field computational imaging of pathology slides using lens-free on-chip microscopy. *Sci Transl Med* 2014; **6**: 267ra175.
21 Bishara W, Su TW, Coskun AF, Ozcan A. Lensfree on-chip microscopy over a wide field-of-view using pixel super-resolution. *Opt Express* 2010; **18**: 11181–11191.
22 Mudanyali O, Oztoprak C, Tseng D, Erlinger A, Ozcan A. Detection of waterborne parasites using field-portable and cost-effective lensfree microscopy. *Lab Chip* 2010; **10**: 2419–2423.
23 Greenbaum A, Luo W, Khademhosseinieh B, Su TW, Coskun AF *et al*. Increased space-bandwidth product in pixel super-resolved lensfree on-chip microscopy. *Sci Rep* 2013; **3**: 1717.
24 McLeod E, Luo W, Mudanyali O, Greenbaum A, Ozcan A. Toward giga-pixel nanoscopy on a chip: a computational wide-field look at the nano-scale without the use of lenses. *Lab Chip* 2013; **13**: 2028–2035.
25 Fienup JR. Reconstruction of an object from the modulus of its Fourier transform. *Opt Lett* 1978; **3**: 27–29.
26 Fienup JR. Phase retrieval algorithms: a comparison. *Appl Opt* 1982; **21**: 2758–2769.
27 Allen LJ, Oxley MP. Phase retrieval from series of images obtained by defocus variation. *Opt Commun* 2001; **199**: 65–75.
28 Zhang Y, Pedrini G, Osten W, Tiziani HJ. Whole optical wave field reconstruction from double or multi in-line holograms by phase retrieval algorithm. *Opt Express* 2003; **11**: 3234–3241.
29 Almoro P, Pedrini G, Osten W. Complete wavefront reconstruction using sequential intensity measurements of a volume speckle field. *Appl Opt* 2006; **45**: 8596–8605.
30 Kanka M, Riesenberg R, Petruck P, Graulig C. High resolution (NA=0.8) in lensless in-line holographic microscopy with glass sample carriers. *Opt Lett* 2011; **36**: 3651–3653.
31 Schwarz CJ, Kuznetsova Y, Brueck SRJ. Imaging interferometric microscopy. *Opt Lett* 2003; **28**: 1424–1426.
32 Mico V, Zalevsky Z, Garcia-Martinez P, Garcia J. Single-step superresolution by interferometric imaging. *Opt Express* 2004; **12**: 2589–2596.
33 Alexandrov SA, Hillman TR, Gutzler T, Sampson DD. Synthetic aperture Fourier holographic optical microscopy. *Phys Rev Lett* 2006; **97**: 168102.
34 Mico V, Zalevsky Z, García J. Superresolution optical system by common-path interferometry. *Opt Express* 2006; **14**: 5168–5177.
35 Mico V, Zalevsky Z, García-Martínez P, García J. Superresolved imaging in digital holography by superposition of tilted wavefronts. *Appl Opt* 2006; **45**: 822–828.
36 Mico V, Zalevsky Z, García-Martínez P, García J. Synthetic aperture superresolution with multiple off-axis holograms. *J Opt Soc Am A* 2006; **23**: 3162–3170.
37 Ralston TS, Marks DL, Carney PS, Boppart SA. Interferometric synthetic aperture microscopy. *Nat Phys* 2007; **3**: 129–134.
38 Martínez-León L, Javidi B. Synthetic aperture single-exposure on-axis digital holography. *Opt Express* 2008; **16**: 161–169.
39 Granero L, Micó V, Zalevsky Z, García J. Synthetic aperture superresolved microscopy in digital lensless Fourier holography by time and angular multiplexing of the object information. *Appl Opt* 2010; **49**: 845–857.
40 Micó V, Zalevsky Z. Superresolved digital in-line holographic microscopy for high-resolution lensless biological imaging. *J Biomed Opt* 2010; **15**: 046027.
41 Rodrigo JA, Alieva T, Cristóbal G, Calvo ML. Wavefield imaging *via* iterative retrieval based on phase modulation diversity. *Opt Express* 2011; **19**: 18621–18635.
42 Tippie AE, Kumar AK, Fienup JR. High-resolution synthetic-aperture digital holography with digital phase and pupil correction. *Opt Express* 2011; **19**: 12027–12038.
43 Pelagotti A, Paturzo M, Locatelli M, Geltrude A, Meucci R *et al*. An automatic method for assembling a large synthetic aperture digital hologram. *Opt Express* 2012; **20**: 4830–4839.
44 Zheng G, Horstmeyer R, Yang C. Wide-field, high-resolution Fourier ptychographic microscopy. *Nat Photonics* 2013; **7**: 739–745.
45 Tian L, Li X, Ramchandran K, Waller L. Multiplexed coded illumination for Fourier Ptychography with an LED array microscope. *Biomed Opt Express* 2014; **5**: 2376–2389.
46 Fienup JR. Reconstruction of a complex-valued object from the modulus of its Fourier transform using a support constraint. *J Opt Soc Am A* 1987; **4**: 118–123.
47 Mudanyali O, Tseng D, Oh C, Isikman SO, Sencan I *et al*. Compact, light-weight and cost-effective microscope based on lensless incoherent holography for telemedicine applications. *Lab Chip* 2010; **10**: 1417–1428.
48 Hardie RC, Barnard KJ, Bognar JG, Armstrong EE, Watson EA. High-resolution image reconstruction from a sequence of rotated and translated frames and its application to an infrared imaging system. *Opt Eng* 1998; **37**: 247–260.
49 Elad M, Hel-Or Y. A fast super-resolution reconstruction algorithm for pure translational motion and common space-invariant blur. *IEEE Trans Image Process* 2001; **10**: 1187–1193.
50 Park SC, Park MK, Kang MG. Super-resolution image reconstruction: a technical overview. *IEEE Signal Process Mag* 2003; **20**: 21–36.
51 Farsiu S, Elad M, Milanfar P. Multiframe demosaicing and super-resolution of color images. *IEEE Trans Image Process* 2006; **15**: 141–159.
52 Pech-Pacheco JL, Cristobal G, Chamorro-Martinez J, Fernandez-Valdivia J. Diatom autofocusing in brightfield microscopy: a comparative study. Proceedings of the 15th International Conference on Pattern Recognition 2000. Barcelona, Spain September 3-7, 2000. IEEE Computer Society: Los Alamitos, CA, USA, 2000.
53 Goodman J. *Introduction to Fourier Optics*. 3rd ed. Greenwood Village, CO: Roberts and Company Publishers; 2004.
54 Greenbaum A, Feizi A, Akbari N, Ozcan A. Wide-field computational color imaging using pixel super-resolved on-chip microscopy. *Opt Express* 2013; **21**: 12469–12483.
55 Levin A, Lischinski D, Weiss Y. Colorization using optimization. *ACM Trans Graph* 2004; **23**: 689–694.
56 Gonzalez RC. *Digital Image Processing*. 3rd ed. Upper Saddle River, NJ: Prentice Hall; 2008.
57 Zernike F. Phase contrast, a new method for the microscopic observation of transparent objects. *Physica* 1942; **9**: 686–698.
58 Gorocs Z, Ozcan A. On-chip biomedical imaging. *IEEE Rev Biomed Eng* 2013; **6**: 29–46.

**This work is licensed under a Creative Commons Attribution-NonCommercial-NoDerivs 3.0 Unported License. The images or other third party material in this article are included in the article's Creative Commons license, unless indicated otherwise in the credit line; if the material is not included under the Creative Commons license, users will need to obtain permission from the license holder to reproduce the material. To view a copy of this license, visit http://creativecommons.org/licenses/by-nc-nd/3.0/**